Published in final edited form as:
Biomaterials. 2013 December ; 34(38): 10007–10015. doi:10.1016/j.biomaterials.2013.09.039.

A Biodegradable Microvessel Scaffold as a Framework to Enable Vascular Support of Engineered Tissues

Xiaofeng Ye[1], **Liang Lu**[1], **Martin E. Kolewe**[1], **Hyoungshin Park**[2], **Benjamin L. Larson**[1], **Ernest S. Kim**[2], and **Lisa E. Freed**[1,2,*]

[1]Harvard-MIT Division of Health Sciences and Technology, David H. Koch Institute for Integrative Cancer Research, and Institute for Medical Engineering and Science, Massachusetts Institute of Technology, Cambridge, MA, 02139 USA

[2]Microsystems Development Group, Charles Stark Draper Laboratory, Cambridge, MA, 02139 USA

Abstract

A biodegradable microvessel scaffold comprised of distinct parenchymal and vascular compartments separated by a permeable membrane interface was conceptualized, fabricated, cellularized, and implanted. The device was designed with perfusable microfluidic channels on the order of 100 μm to mimic small blood vessels, and high interfacial area to an adjacent parenchymal space to enable transport between the compartments. Poly(glycerol sebacate) (PGS) elastomer was used to construct the microvessel framework, and various assembly methods were evaluated to ensure robust mechanical integrity. *In vitro* studies demonstrated the differentiation of human skeletal muscle cells cultured in the parenchymal space, a 90% reduction in muscle cell viability due to trans-membrane transport of a myotoxic drug from the perfusate, and microvessel seeding with human endothelial cells. *In vivo* studies of scaffolds implanted subcutaneously and intraperitoneally, without or with exogenous cells, into nude rats demonstrated biodegradation of the membrane interface and host blood cell infiltration of the microvessels. This modular, implantable scaffold could serve as a basis for building tissue constructs of increasing scale and clinical relevance.

1. Introduction

A major factor impeding the clinical translation of tissue-engineered constructs that include cells in combination with various biomaterial substrates is the limited size of functional tissue that can be produced. More specifically, preventing cell death at the center of thick constructs during *in vitro* culture and in the initial phase post-implantation will require readily perfusable microvessels, due to the limited diffusion distance of oxygen and the slow physiological rate of new blood vessel growth [1–4]. A support system, such as integrated microvessels, and a strategy for graft-host vascular integration are needed to sustain large viable engineered tissues with demanding oxygen and nutrient requirements, such as muscle.

*Corresponding author: Freed, L.E. Microsystems Development Group, C.S. Draper Laboratory and MIT-Affiliated Research Scientist, 555 Technology Square-Mail Stop 32, Cambridge, MA 02139-4307 USA. Tel: (617) 258-4234; Fax: 617-258-3858; Lfreed@draper.com, Lfreed@mit.edu.

Recent advances in photolithography, 3D printing, and 3D sacrificial molding technologies have recapitulated functional, vascular-like structures in both degradable [1, 2, 5, 6] and non-degradable [7–10] materials. However, previous microfluidic devices focused on the vascular compartment [7, 11–13] and/or required non-degradable materials such as poly(dimethyl siloxane)(PDMS) [7, 14–16]. Previous studies have not yet demonstrated a robustly perfusable, implantable scaffold that enables vascular—parenchymal transport via a degradable interface.

Scaffolds with pre-formed microvasculatures derived from cultured cells (endothelial or progenitor) can integrate with host blood vessels [4] and accelerate the functional integration of skeletal muscle grafts *in vivo* [3]. However, vascular integration after *in vivo* implantation required a period of several days to weeks, both for decellularized small intestinal submucosa (SIS) [3] and porogen-leached polymers such as poly(L-lactic acid) (PLLA) and poly (lactic-co-glycolic acid) (PLGA) [17, 18]. This timeframe is too long to allow survival of complex tissue constructs with high metabolic requirements; these will require immediate perfusion, as is the state of the art for large plastic and reconstructive allografts [19].

As an alternative to decellularized tissue and polymers with randomly structured pores (e.g., PLGA sponges), scaffolds with engineered microvasculature could enable host-graft vascular integration both at the micro-scale and, with scale-up of inlet and outlet, allow immediate perfusion by direct anastomosis to host arteries and veins. Moreover, biomaterials from the class of a polyol sebacate polymers, which includes PGS [20, 21], could be fabricated into mechanically competent framework of compartments and semi-permeable interfaces, in contrast to hydrogels, which by comparison are generally weaker, or thermoplastic polymers (e.g., PLGA), which by comparison are generally too stiff.

Poly(glycerol sebacate) was strategically designed to combine rubber-like elasticity, strength, and rapid biodegradation by surface erosion to enable rapid tissue remodeling and repair [22, 23]. Biocompatibility of PGS was shown for all cell types found in muscle, including cardiac [24–30], and skeletal [31], myocytes and endothelial cells [11, 23, 32, 33]. Moreover, mechanical properties and biodegradation rate of members of the polyol sebacate family can be controlled by varying monomer composition [34], curing time [26], and curing temperature [35]. Moreover, PGS can be precisely fabricated to achieve high aspect ratio features (150 μm height, 30 μm width) and 3D scaffold architectural structures by combining Si wafer micromolding [28] with semi-automated layer-by-layer alignment and bonding [29]. However, while previous studies have shown meso-scale muscle fiber development on 3D porous PGS scaffolds, a perfusable, implantable multi-compartmental PGS scaffold has not been previously demonstrated.

In the present study, a biodegradable scaffold with parenchymal and vascular compartments separated by a permeable membrane was fabricated from PGS. Scaffolds were cellularized and characterized with human skeletal muscle cells and endothelial cells *in vitro*, then implanted with and without cells *in vivo*. Analyses of trans-membrane transport, membrane biodegradation, and host blood cell infiltration of the microvessels were performed to evaluate the suitability of this scaffold as a framework to support large engineered tissues.

2. Materials and Methods

2.1. Design

The microfluidic device base (μFD base) had a simple design, with 250 μm inner diameter inlet and an outlet channels, a 4 cm^2 square central area comprising 150 parallel microchannels, and a boat-shaped footprint (Figure 1). Arrays of ~100 μm diameter posts were placed at 250 μm intervals at the inlet and outlet in order to provide structural integrity

[36] and help distribute flow (Figure 1 B1). Long, transitional entrance and exit regions [37] further aided in the distribution of flow to all of the central channels (Figure 1 B2). The central channels, each 2 cm long, 100 μm wide, and 100 μm high, were separated by 30 μm wide ribs (Figure 1 B3). This design considered both 2D (in-plane) fluid flow and trans-membrane (out-of-plane) area available for transport to an adjacent parenchymal space in the context of a device with a sufficiently large working area to allow for the generation of reliable replicates for *in vitro* and *in vivo* studies. Dimensions of the inlet, outlet, and central channels were selected to be within the size range of natural vasculature [38]; flow rate was empirically selected to maintain steady channel filling and perfusion. Overall, our channel dimensions were similar to those in a recently reported device [7] that was designed based on mathematical modeling, made of PDMS and glass, and used to create an endothelial cell-based microcirculatory network.

2.2. Scaffold fabrication

Etched Si wafers (100 mm diameter, 1 mm thick, WRS Materials, San Jose, CA) were used as molds for the PGS μFD base. Wafers were coated with hexamethyldisilazane and UV exposure was applied through a 20,000 dpi Mylar mask transparency, the design for which was laid out using L-Edit software (Tanner, San Jose, CA) [31]. Wafers were then developed, rinsed, dried, oxygen plasma (OP) treated, and hard baked. Exposed Si was then etched to a target depth of 150 μm using an inductively coupled plasma etcher (STS-ICP, Newport, UK); the photoresist was stripped, and wafers were cleaned in a Piranha bath (1:1 H_2SO_4: H_2O_2), rinsed and dried. Wafers were then subjected to isotropic etch (STS RIE, Newport, UK) to smooth sidewalls and corners [28]. After another OP treatment and Piranha clean, wafers were stored until use. To facilitate PGS molding, wafers were spin-coated with a sacrificial layer of maltose (70% w/v in DI water) [28] and then post-baked and stored with desiccant at room temperature (RT) until use.

The PGS pre-polymer was synthesized by reacting a 1:1 molar ratio of glycerol and sebacic acid under heat and vacuum [22, 28]. The PGS μFD base was micromolded by volumetric casting and curing of the pre-polymer in the etched Si wafer in a vacuum oven (165°C, 40 mTorr) [28]. To provide a thin PGS membrane to cover the μFD base, pre-polymer (50% w/v in ethanol) was cast on an unpatterned maltose coated Si wafer followed by heating and vacuum curing. The PGS μFD base and membrane were peeled off the wafers, subjected to graded ethanol washes (of up to 50% v/v in DI water to remove unreacted oligomer), and rinsed. Narrow slits were cut at the inlet and outlet of the μFD base to allow in-line insertion of coated silica inlet and outlet tubing for device perfusion (200026-10M, TSP250360, Molex Connector Group, Wooster, OH).

To assemble closed channels from a μFD base and a membrane, three bonding methods were explored: (i) OP, (ii) 3-aminopropyltriethoxysilane (APTES), and (iii) PGS solvent bonding. For OP bonding, a membrane cured for 8 h was OP-treated (100 W, 120 s) and held in contact with a μFD base cured for 16 h. For APTES bonding, a membrane cured for 8 h was OP-treated, sprayed with APTES (5% w/v in DI water), heated for 20 min at 80°C, and held in contact with an OP-treated μFD base cured for 16 h. For PGS solvent bonding, a thin layer of PGS pre-polymer (25% w/v in ethanol) was heated on an unpatterned Si wafer for 30 min at 110°C and transferred by dip-coating to the patterned side of a μFD base cured for 14 h. Next, a membrane cured for 6 h was held in contact with the dip-coated μFD base, and the resulting composite device was re-cured for an additional 2 h. To provide parenchymal chambers, four PDMS gaskets (8 mm inner diameter, 6 mm high) were attached to the PGS membrane above the central microvessels using silicone adhesive (3140, Dow Corning, Midland, MI). Prior to use with cells, assembled devices were autoclave-sterilized (121°C for 30 min on a wet cycle).

2.3. Scanning electron microscopy (SEM)

The SEM analysis was as previously described [31]. Briefly, full-thickness cross-sections of specimens were harvested from the central region of the microvessel scaffold, dried, sputter coated with gold-palladium, and imaged using a S3500 Hitachi SEM (High Technologies America).

2.4. Mechanical testing

Mechanical testing was similar to our previous studies [26, 28]. Dry full-thickness cross-specimens were prepared from the central region of the scaffold using a dog-bone punch (gauge length 5 mm, width 2 mm) oriented in parallel to the microvessels. Samples were mounted on a mechanical tester (ELF 3200 Bose, Framingham, MA) fitted with a 250 g load cell (Sensotech, Inc., Columbus, OH) and strained to failure at 2% strain/s. Effective stiffness was calculated from the slope of the stress–strain curve between 1% and 10% strain; ultimate tensile stress (UTS) and the first strain-to-failure (εf) were also calculated from the stress-strain curve.

2.5. Flow testing

A syringe filled with phosphate buffered saline (PBS) was attached to the device inlet, an empty syringe was attached to the device outlet, and the device was subjected to unidirectional flow using a push-pull syringe pump (PHD RS485, Harvard Apparatus). Devices were tested at flow rates of 10 μL/min and 100 μL/min for up to five days; any detachment between the two layers indicated by macroscopic visual observation was considered as failure of the bond. Flow visualization studies were done in the same setup, using 50% v/v eosin-Y DI water (HT110280, Sigma, St. Louis, MO) or fluorescently labeled 10 μm diameter microspheres at 0.1% (w/v) in PBS (18140, Polysciences, Warrington, PA). Images were recorded using a Zeiss Axiovert 200M epifluorescence microscope equipped with a video camera (Sony, XCD-X710).

2.6. In vitro studies

Adult human skeletal muscle derived cells (hSkMDCs) [39] were obtained from Cook Myosite Inc. (CMI, Pittsburgh, PA). The hSkMDCs were expanded in growth medium (MB-2222, CMI) according to manufacturer's instructions. The PGS membrane was pre-treated by pipetting 400 μL of 10 μg/mL fibronectin (F0895, Sigma, St. Louis, MO) into each of the four upper chambers and incubating overnight at 37°C, after which passage 5 hSkMDCs were seeded (5×10^4 cells and 400 μL of growth medium per chamber). After 24 h, the hSkMDCs growth medium was replaced with differentiation medium (MD-5555, CMI) and microvessel perfusion was initiated. A syringe filled with differentiation medium was placed on the push-pull pump and attached to the inlet of the device via a gas exchanger (508-005 Cole Parmer silicone rubber tubing, 50 cm long, 2.16 mm OD, 1.02 mm ID, and 0.67 mm wall). Unidirectional push-pull flow was established at 10 μL/min, and the system was placed in a standard cell culture incubator. The medium in the syringes was replaced every two days. After five days, full thickness specimens were harvested, one from each chamber, using an 8 mm diameter dermal punch (P850, Acuderm, Ft. Lauderdale, FL). Glass coverslip cultures of hSkMDCs provided controls.

In other studies, the microvessel perfusate was supplemented with 50 μM doxorubicin (DOX) (2252, TORIS Bioscience, Bristol, UK), a drug with known myotoxic side effects [40, 41], while hSkMDCs were cultured in the parenchymal space. Microvessel perfusion without DOX served as one set of controls while petri dish cultures of hSkMDCs provided a second set of controls. After five days of culture, hSkMDCs viability was examined using three commercial kits according to manufacturers' instructions. For the CellTiter-Glo™

assay (G7570, Promega, Madison, WI), hSkMDCs cultures were incubated for 10 min at RT with a reagent that produced a fluorescent signal proportional to the amount of ATP present and assessed using a SpectraFluor Plus (Tecan, Research Triangle Park, NC). For the Live/Dead assay (L3224, Molecular Probes, Eugene, OR), hSkMDCs cultures were incubated for 45 min at RT with 4 μM calcein-AM and 2 μM ethidium homodimer, then imaged using a Zeiss Axiovert 200M epifluorescence microscope. Apoptosis was detected after fixing specimens in 10% neutral buffered formalin (NBF), embedding in paraffin, and sectioning to 5 μm, using the terminal deoxynucleotidyl transferase–mediated dUTP nick end labeling (TUNEL) assay (4828-30-BK, R&D Systems, Gaithersburg, MD).

In other studies, microvessels of devices were seeded with human umbilical vein endothelial cells (HUVECs) after culturing hSkMDCs in the parenchymal space. The HUVECS (ATCC PCS-100-030) were expanded in basal medium (ATCC PCS-100-030) containing endothelial cell growth kit-BBE (ATCC PCS-100-040). Passage 4 HUVECs were infused into the microvessels (1.2×10^7 cells per 300 μL) using a push-pull pump at 25 μL/min. Specimens were cultured statically overnight; to minimize evaporative loss, medium was added to a well created by a PDMS gasket to create a thin layer of fluid over the entire top surface of the device.

2.7. In vivo *studies*

Immunodeficient rats (n=8 males, 8 weeks old, 200–250 g, NIH RNU, Charles River) were used following the guidance of the NIH and an Institutional Animal Care and Use Committee. Microvessel scaffolds were implanted at two sites, subcutaneous (SC) and intraperitoneal (IP), in four experimental groups: (i) SC without cells, (ii) SC with exogenous cells, (iii) IP without cells, and (iv) IP with exogenous cells, and there were four to six replicates per group. In groups (ii) and (iv), hSkMDCs were seeded in the parenchymal space and cultured in differentiation medium for three days, then HUVECs were seeded in the vascular space and incubated overnight, as described in Section 2.6. In all four groups, 8 mm diameter, full thickness discs of the microvessel scaffold were die-punched, subdivided into halves or thirds, and implanted. The SC implants were inserted without fixation into dorsal pouches, while IP implants were fixed onto the mesentery of the small intestine using a single loose suture made of 6-0 prolene. One rat was euthanized after one day due to a post-operative complication, four rats with SC and IP implants were euthanized after 1 week, one rat with IP implants was euthanized after 2 weeks, and two rats with SC implants were euthanized after 4 weeks.

2.8. Histological analyses

At the conclusion of *in vitro* cultures, full-thickness specimens were harvested from devices using a dermal punch; *in vivo* explants were harvested en-bloc following euthanasia. Specimens designated for histological staining were fixed in 10% NBF, embedded in paraffin, and sectioned to either 20 μm or 5 μm, for *in vitro* or *in vivo* studies respectively. Specimens designated for immunostaining and cryosectioning were fixed in 10% NBF, embedded in Tissue Tek O.C.T. compound, sectioned (20 μm), rinsed, and permeabilized in Triton X-100 (Sigma), 0.2% (v/v) in PBS for 0.5 h. Fluorescein isothiocyanate (FITC)-phalloidin conjugate was used to detect F-actin (Sigma P5282; 1:200 dilution factor (df)).

For *in vitro* studies, hSkMDCs were immunostained for F-actin, desmin, and sarcomeric α-actin, and HUVECs were immunostained with von Willebrand's Factor (vWF). The primary antibodies were: anti-human sarcomeric α-actin antibody (Sigma A7811; 1:200 df), anti-human desmin antibody (Dako Clone D33; 1:200 df) and anti-human vWF (Sigma F3520; 1:200 df). After incubating with a fluorescein-conjugated secondary IgG antibody (1:200 df), specimens were rinsed, incubated in mounting medium with DAPI (Vector laboratories

H-1200), cover-slipped, and imaged using a MICF-Nikon 1AR Ultra-Fast Spectral Scanning Laser Confocal Microscope.

For *in vivo* studies, the primary antibodies were monoclonal anti-rat CD31 antibody (Abcam ab7388; 1:200 df), which provided marker for host rat endothelial cells, and anti-human human specific nuclear antigen antibody (MAB1281; Millipore, Temecula, CA, 1:200 df) which provided a marker for exogenous human cells. Other specimens were paraffin-embedded and stained with hematoxylin and eosin (H&E). To assess thickness of the PGS membrane interface, regions of interest above individual microchannels were defined using Image-J, and thickness was calculated as measured area divided by width and expressed as percent of thickness at time-zero for at least six microchannels within representative samples from each group.

2.9. Statistical analyses

Multi-way analysis of variance was performed in conjunction with Tukey's *post hoc* test using SPSS version 21.0. Values of $p < 0.05$ were considered statistically significant.

3. Results

3.1. Structural and mechanical characterization of assembled scaffolds

A PGS μFD base was replica-molded off an etched silicon wafer and tightly bonded to a PGS membrane to create a closed microfluidic device as shown schematically and in micrographs in Figure 1 and Figure 2A–F. Structural and functional (mechanical and flow) testing were used to select the best bonding technique for "microvessel scaffolds" assembled using three different methods: OP, APTES and PGS solvent bonding (Figure 2, Table 1, Supplemental Data 1, Supplemental Videos 1–3). Seamless bonding, as assessed by cross-sectional SEM, was found only in the PGS solvent bonding group (compare Figure 2F with Figures 2B and 2D). The SEM analyses also showed that feature sizes of the microchannels were consistent with the dimensions of the etched Si wafer (depth of ~100 μm, height of ~100 μm deep, and rib width of ~30 μm), while the thicknesses of the μFD base and membrane were respectively ~175-to-185 μm and ~100-to-120 μm.

Scaffolds in the PGS solvent bonding group did not fail over five days of perfusion at lower and higher flow rates of 10 and 100 μL/min (Table 1), in contrast to the OP and APTES bonding groups where most of the devices failed at the lower rate within 4 h. The UTS was higher for PGS solvent bonding group than either OP or APTES bonding (Figure 2G). Stress versus strain curves revealed a single failure point for the PGS solvent bonding group, indicating that the μFD base remained firmly bonded to the membrane until failure, whereas serial failure of first the μFD and then the membrane in the OP and APTES groups suggested their bonds were less robust (Supplemental Data 1). Effective stiffness was higher for PGS solvent and APTES bonding than for OP bonding (Figure 2H). The initial value of failure strain was in the range of 0.4 to 0.5 and was similar for all three bonding methods (Figure 2I). Based on SEM imaging and flow and mechanical test data, PGS solvent bonding was used for scaffold assembly in all further studies.

Flow visualization studies using tracer dyes and microsphere particles showed flow patterns resembling plug flow, without aggregation or adherence of particles to channels walls (Supplemental Videos 1–3).

3.2. In vitro studies

In vitro studies of hSkMDCs differentiation in the parenchymal compartment, trans-membrane transport of a myotoxic drug, and seeding of HUVECs into the microvessels are

shown schematically in Figure 3 and results are demonstrated in Figures 4–6. In all cases, *in vitro* studies were carried out in an incubator-compatible circuit, using a syringe pump connected to a gas exchanger to perfuse the microvessels, while hSkMDCs were cultured in four parenchymal chambers on top of the membrane.

Over five days of culture, the hSkMDCs fused into multi-nucleated myotubes (Figure 4C). Elongated cell structures were demonstrated by F-actin staining (Figure 4A) and differentiation was demonstrated by immunostaining for desmin (Figure 4B) and sarcomeric α-actin (Figure 4D). While hSkMDCs cultured on PGS scaffolds were less elongated and exhibited less developed sarcomeres than control cultures on glass coverslips (Figures 4E–H), the scaffolds clearly supported human myocyte growth and differentiation.

Trans-membrane transport was demonstrated by about 90% reduction in hSkMDCs viability in the parenchymal compartment due to transport of a myotoxic drug (DOX, 578 Da) from the perfusate within the vascular compartment. The CellTiter Glo kit (Figure 5A), Live/Dead staining (Figure 5C) and TUNEL assays (Figure 5G) all demonstrated high numbers of dead and apoptotic hSkMDCs, and H&E stain revealed loss of cell integrity (Figure 5F) when the perfusate contained DOX. In contrast, hSkMDCs viability as assessed by these same indexes was high when the perfusate did not contain DOX (Figures 5 A, B, E). The CellTiter Glo kit also showed about 90% reduction in viability for hSkMDCs cultured in Petri dishes using medium that contained DOX (Figure 5A).

Another study demonstrated the feasibility of seeding microvessels with HUVECs, albeit without optimization of cell concentration, adhesion or spreading (Figure 6). Presence of HUVECs was demonstrated by vWF immunostaining (Figure 6 B1, C1); however, the cells appeared rounded and were sparsely distributed at the bottoms of the channels. Co-staining with vWF and F-actin confirmed that HUVECs were located in the microvessels while hSkMDCs were located in the parenchymal space (Figure 6 B, C).

3.3. In vivo studies

Scaffold biodegradation in association with microchannel vascularization were clearly demonstrated *in vivo*, one week after implanting full-thickness punches of scaffolds without or with exogenous cells into nude rats (Figure 3 and Figure 7). Initial wet weights, thicknesses, and surface areas of the implants were about 5-to-7 mg, 300 μm, and 0.35-to-0.50 cm^2, respectively.

Interfacial membrane degradation was quantified (Figure 7K) by comparing H&E stained cross-sections of the four groups of one-week implants to initial (time-zero) implants. There were significant effects of time and presence of exogenous cells on membrane biodegradation at both sites. In the group where degradation was most rapid, membrane thickness was reduced to 39% of its initial value within one week. At later time points (two and four weeks), implants could not be found and were presumed to have completely biodegraded.

The cells within the microvessels of one-week explants (Figure 7C–E) were determined to be host cells by immunostaining for rat CD31 (Figure 7 G–J); a CD-31 stained normal rat microvessel provided a positive control (Figure 7F). The H&E and CD-31 staining patterns showed consistent trends from group to group, with IP implants with exogenous cells exhibiting the most rapid membrane biodegradation and vascularization (Figure 7 I–K). Erythrocytes were present in the microvessels of IP implants with exogenous cells, as shown in a representative H&E stained longitudinal section (Figure 7L).

4. Discussion

Biomaterial microfabrication by Si-based micromolding [13], additive manufacturing [42], and layer-by-layer assembly [29] holds promise for tissue engineering and regenerative medicine. Toward building tissues with integrated vasculatures, we designed and fabricated a scalable unit comprised of adjacent microvessel and parenchymal compartments, demonstrated spatially organized cell populations and inter-compartmental transport in association with microvessel perfusion *in vitro*, and confirmed biodegradation of the membrane interface in association with host blood cell infiltration of the microvessels *in vivo*.

The design of our microvasculature allowed 2D (in-plane) perfusion in a pattern resembling plug flow while also providing a higher area for trans-membrane (out-of-plane) transport than previously reported designs based on successive generations of bifurcating microchannels [9, 13]. More specifically, our transport area was 77% for 100 μm high × 100 μm wide channels with center-to-center spacing of 130 μm, whereas in a recent report [9] the transport area in the area of the smallest channels fabricated (200 μm high × 200 μm wide with center-to-center spacing of 400 μm) was lower (50%). It will be interesting to directly compare microvessel scaffolds fabricated by Si-based micromolding and additive manufacturing, and find ways to combine these promising bioMEMS technologies.

Continuous microvessel perfusion under standard *in vitro* culture conditions for five days was made possible by a mechanically stable bond between the two device layers. Only the chemical cross-linkage created by PGS solvent bonding (dip-coating a μFD base into a solution of a pre-polymer and then bringing the base into contact with a membrane followed by vacuum curing) yielded a robustly perfusable device, in contrast to OP, previously shown to bond two layers of PGS scaffolds not used for perfusion [27] and APTES, previously shown to bond polymer membranes to PDMS or glass [43].

In vitro studies showed that perfusing the microvessels with DOX had cytotoxic effects on hSkMDCs in the parenchymal space [40, 41]. While the current interfacial material may eventually need to be replaced with something more permeable, and drainage or lymphatics need to be added [5] the present findings showed trans-membrane transport in the context of a fully degradable device. *In vitro* studies also demonstrated differentiation of hSkMDCs cultured on scaffolds, but cells were less elongated and sarcomeres less developed than controls cultured on glass coverslips suggesting that myogenesis remained incomplete under the conditions tested. Consistent with findings previously reported for PDMS microdevices [7], our study of PGS microdevices highlighted the need to remove un-crosslinked oligomer (sol). More specifically, perfusion caused hSkMDCs death when microvessel scaffolds were not pre-treated with ethanol, and this problem was resolved by pre-incubating device components in ethanol prior to cell culture. Interestingly, cytotoxicity was not previously observed in our studies of PGS scaffolds that were neither pre-treated in ethanol nor perfused [28, 29].

In vivo studies showed degradation of the interfacial membrane, suggesting the approach may eventually be used enable direct contact between cells of different types organized in adjacent device compartments. Membrane degradation was associated with host blood cell infiltration of the microvessels and, in the fastest degrading group–IP implanted scaffolds with exogenous cells– membrane thickness was reduced to 39% of its initial value over one week. Possible explanations for why the presence of exogenous cells was associated with faster membrane biodegradation and more extensive graft-host vascular integration include release by exogenous cells of enzymes such as lipase that can degrade PGS [42] and/or hypoxia-inducible-factor-1alpha which can induce the release of pro-angiogenic growth

factors [4]. The inflammatory response to the surgical wound and foreign materials (*i.e.*, human cells and/or PGS) appeared to be minimal in our immunocompromised hosts.

Rapid biodegradation of the scaffolds by surface erosion can be attributed to their small mass, high surface-to-volume ratio geometry, and the polymer curing conditions (high temperature, short duration), as compared to other *in vivo* studies of PGS implants [44–46]. It will be interesting to selectively control the rates of degradation of the individual scaffold components by using biomaterials with various chemical compositions, processing conditions, and geometries.

Further work is needed to improve the scaffold's capacity for exogenous cell delivery. Human SkMDCs were not detectable in one-week explants, presumably due to their detachment from the scaffold in association with the implantation process; in the next prototype device, a porous scaffold will be integrated into the parenchymal space in an effort to increase muscle cell retention. Although host-derived vascular structures were present in one-week explants, further work can be done to improve the attachment and distribution of exogenous endothelial cells, including microchannel pre-treatment with fibronectin and device rotation during cell seeding which enabled 3D endothelialization of 100 μm × 200 μm rectangular channels made of PDMS [7].

5. Conclusion

We conceptualized, fabricated, cellularized, and implanted a mechanically robust, elastomeric, biodegradable microvessel scaffold with distinct vascular and parenchymal compartments separated by a permeable membrane. The microvessel scaffold supported the *in vitro* cultivation of hSkMDCs in its parenchymal space. Trans-membrane transport was proven by inducing death of parenchymal hSkMDCs by perfusing a myotoxic drug through the microvessels. Substantial biodegradation of the membrane in association with host blood cell infiltration of the microvessels occurred within one week of device implantation *in vivo*. Together, these findings demonstrate an implantable, scalable unit that can be populated with exogenous and/or host cells in a spatially organized manner and, with further development, may address the clinical need for a large engineered tissue grafts with a readily perfusable, integrated microvasculature.

Supplementary Material

Refer to Web version on PubMed Central for supplementary material.

Acknowledgments

This work was funded by the National Heart, Lung and Blood Institute (NHLBI), Award 1-R01-HL107503 (LEF). The content is solely the responsibility of the authors and does not necessarily represent the official views of the NHLBI or NIH. We thank R. Langer for general advice, M. Guillemette and V. Kolachalama for many helpful discussions, B. Chandapillai, P. Wu and S. Jain for help with preliminary device testing, and J. Hsaio and M. Bancu for help with MEMS Fabrication.

References

1. Miller JS, Stevens KR, Yang MT, Baker BM, Nguyen DH, Cohen DM, et al. Rapid casting of patterned vascular networks for perfusable engineered three-dimensional tissues. Nat Mater. 2012; 11:768–774. [PubMed: 22751181]
2. Bae H, Puranik AS, Gauvin R, Edalat F, Carrillo-Conde B, Peppas NA, et al. Building vascular networks. Sci Transl Med. 2012; 4:160ps23.

3. Koffler J, Kaufman-Francis K, Shandalov Y, Egozi D, Pavlov DA, Landesberg A, et al. Improved vascular organization enhances functional integration of engineered skeletal muscle grafts. Proc Natl Acad Sci U S A. 2011; 108:14789–14794. [PubMed: 21878567]
4. Laschke MW, Vollmar B, Menger MD. Inosculation: connecting the life-sustaining pipelines. Tissue Eng Part B Rev. 2009; 15:455–465. [PubMed: 19552605]
5. Wong KH, Truslow JG, Khankhel AH, Chan KL, Tien J. Artificial lymphatic drainage systems for vascularized microfluidic scaffolds. J Biomed Mater Res A. 2013; 101:2181–2190. [PubMed: 23281125]
6. Bellan LM, Pearsall M, Cropek DM, Langer R. A 3D interconnected microchannel network formed in gelatin by sacrificial shellac microfibers. Adv Mater. 2012; 24:5187–5191. [PubMed: 22826135]
7. Chau LT, Rolfe BE, Cooper-White JJ. A microdevice for the creation of patent, three-dimensional endothelial cell-based microcirculatory networks. Biomicrofluidics. 2011; 5:34115–3411514. [PubMed: 22662042]
8. Zheng Y, Chen J, Craven M, Choi NW, Totorica S, Diaz-Santana A, et al. In vitro microvessels for the study of angiogenesis and thrombosis. Proc Natl Acad Sci U S A. 2012; 109:9342–9347. [PubMed: 22645376]
9. Hansen CJ, Saksena R, Kolesky DB, Vericella JJ, Kranz SJ, Muldowney GP, et al. High-throughput printing via microvascular multinozzle arrays. Adv Mater. 2013; 25:96–102. [PubMed: 23109104]
10. Wu W, DeConinck A, Lewis JA. Omnidirectional printing of 3D microvascular networks. Adv Mater. 2011; 23:H178–H183. [PubMed: 21438034]
11. Fidkowski C, Kaazempur-Mofrad MR, Borenstein J, Vacanti JP, Langer R, Wang Y. Endothelialized microvasculature based on a biodegradable elastomer. Tissue Eng. 2005; 11:302–309. [PubMed: 15738683]
12. Bettinger CJ, Weinberg EJ, Kulig KM, Vacanti JP, Wang Y, Borenstein JT, et al. Three-dimensional microfluidic tissue-engineering scaffolds using a flexible biodegradable polymer. Adv Mater. 2005; 18:165–169. [PubMed: 19759845]
13. King KR, Wang CCJ, Kaazempur-Mofrad MR, Vacanti JP, Borenstein JT. Biodegradable microfluidics. Advanced Materials. 2004; 16:2007–2012.
14. Carraro A, Hsu WM, Kulig KM, Cheung WS, Miller ML, Weinberg EJ, et al. In vitro analysis of a hepatic device with intrinsic microvascular-based channels. Biomed Microdevices. 2008; 10:795–805. [PubMed: 18604585]
15. Kim HJ, Huh D, Hamilton G, Ingber DE. Human gut-on-a-chip inhabited by microbial flora that experiences intestinal peristalsis-like motions and flow. Lab Chip. 2012; 12:2165–2174. [PubMed: 22434367]
16. Huh D, Leslie DC, Matthews BD, Fraser JP, Jurek S, Hamilton GA, et al. A human disease model of drug toxicity-induced pulmonary edema in a lung-on-a-chip microdevice. Sci Transl Med. 2012; 4:159ra47.
17. Tsigkou O, Pomerantseva I, Spencer JA, Redondo PA, Hart AR, O'Doherty E, et al. Engineered vascularized bone grafts. Proc Natl Acad Sci U S A. 2010; 107:3311–3316. [PubMed: 20133604]
18. Lesman A, Koffler J, Atlas R, Blinder YJ, Kam Z, Levenberg S. Engineering vessel-like networks within multicellular fibrin-based constructs. Biomaterials. 2011; 32:7856–7869. [PubMed: 21816465]
19. Siemionow M, Papay F, Alam D, Bernard S, Djohan R, Gordon C, et al. Near-total human face transplantation for a severely disfigured patient in the USA. Lancet. 2009; 374:203–209. [PubMed: 19608265]
20. Rai R, Tallawi M, Grigore A, Boccaccini AR. Synthesis, properties and biomedical applications of poly(glycerol sebacate) (PGS): A review. Progress in Polymer Science. 2012; 37:1051–1078.
21. Chen QZ, Liang SL, Thouas GA. Elastomeric biomaterials for tissue engineering. Progress in Polymer Science. 2013; 38:584–671.
22. Wang Y, Ameer GA, Sheppard BJ, Langer R. A tough biodegradable elastomer. Nat Biotechnol. 2002; 20:602–606. [PubMed: 12042865]
23. Wu W, Allen RA, Wang Y. Fast-degrading elastomer enables rapid remodeling of a cell-free synthetic graft into a neoartery. Nat Med. 2012; 18:1148–1153. [PubMed: 22729285]

24. Radisic M, Park H, Chen F, Salazar-Lazzaro JE, Wang Y, Dennis R, et al. Biomimetic approach to cardiac tissue engineering: oxygen carriers and channeled scaffolds. Tissue Eng. 2006; 12:2077–2091. [PubMed: 16968150]
25. Radisic M, Park H, Martens TP, Salazar-Lazaro JE, Geng W, Wang Y, et al. Pretreatment of synthetic elastomeric scaffolds by cardiac fibroblasts improves engineered heart tissue. J Biomed Mater Res A. 2008; 86:713–724. [PubMed: 18041719]
26. Engelmayr GC Jr, Cheng M, Bettinger CJ, Borenstein JT, Langer R, Freed LE. Accordion-like honeycombs for tissue engineering of cardiac anisotropy. Nat Mater. 2008; 7:1003–1010. [PubMed: 18978786]
27. Park H, Larson BL, Guillemette MD, Jain SR, Hua C, Engelmayr GC Jr, et al. The significance of pore microarchitecture in a multi-layered elastomeric scaffold for contractile cardiac muscle constructs. Biomaterials. 2011; 32:1856–1864. [PubMed: 21144580]
28. Neal RA, Jean A, Park H, Wu PB, Hsiao J, Engelmayr GC Jr, et al. Three-dimensional elastomeric scaffolds designed with cardiac-mimetic structural and mechanical features. Tissue Eng Part A. 2013; 19:793–807. [PubMed: 23190320]
29. Kolewe, ME.; Park, H.; Gray, C.; Ye, X.; Langer, R.; Freed, LE. 3D Structural Patterns in scalable, elastomeric scaffolds guide engineered tissue architecture. Adv Mater. 2013. Available from URL: http://www.ncbi.nlm.nih.gov/pubmed/23765688
30. Marsano A, Maidhof R, Luo J, Fujikara K, Konofagou EE, Banfi A, et al. The effect of controlled expression of VEGF by transduced myoblasts in a cardiac patch on vascularization in a mouse model of myocardial infarction. Biomaterials. 2013; 34:393–401. [PubMed: 23083931]
31. Guillemette MD, Park H, Hsiao JC, Jain SR, Larson BL, Langer R, et al. Combined technologies for microfabricating elastomeric cardiac tissue engineering scaffolds. Macromol Biosci. 2010; 10:1330–1337. [PubMed: 20718054]
32. Lee EJ, Vunjak-Novakovic G, Wang Y, Niklason LE. A biocompatible endothelial cell delivery system for in vitro tissue engineering. Cell Transplant. 2009; 18:731–743. [PubMed: 19500475]
33. Lee KW, Wang Y. Elastomeric PGS scaffolds in arterial tissue engineering. J Vis Exp. 2011; 50:e2691.
34. Bettinger CJ, Bruggeman JP, Borenstein JT, Langer R. In vitro and in vivo degradation of poly(1,3-diamino-2-hydroxypropane-co-polyol sebacate) elastomers. J Biomed Mater Res A. 2009; 91:1077–1088. [PubMed: 19107786]
35. Chen QZ, Bismarck A, Hansen U, Junaid S, Tran MQ, Harding SE, et al. Characterisation of a soft elastomer poly(glycerol sebacate) designed to match the mechanical properties of myocardial tissue. Biomaterials. 2008; 29:47–57. [PubMed: 17915309]
36. Kniazeva T, Hsiao JC, Charest JL, Borenstein JT. A microfluidic respiratory assist device with high gas permeance for artificial lung applications. Biomed Microdevices. 2011; 13:315–323. [PubMed: 21113664]
37. Lawrence BJ, Devarapalli M, Madihally SV. Flow dynamics in bioreactors containing tissue engineering scaffolds. Biotechnol Bioeng. 2009; 102:935–947. [PubMed: 18949759]
38. Folkman J, Hochberg M. Self-regulation of growth in three dimensions. J Exp Med. 1973; 138:745–753. [PubMed: 4744009]
39. Zheng B, Cao B, Crisan M, Sun B, Li G, Logar A, et al. Prospective identification of myogenic endothelial cells in human skeletal muscle. Nat Biotechnol. 2007; 25:1025–1034. [PubMed: 17767154]
40. Smuder AJ, Kavazis AN, Min K, Powers SK. Doxorubicin-induced markers of myocardial autophagic signaling in sedentary and exercise trained animals. J Appl Physiol. 2013; 115:176–185. [PubMed: 23703114]
41. Yokochi T, Robertson KD. Doxorubicin inhibits DNMT1, resulting in conditional apoptosis. Mol Pharmacol. 2004; 66:1415–1420. [PubMed: 15340041]
42. Sun L, Parker ST, Syoji D, Wang X, Lewis JA, Kaplan DL. Direct-write assembly of 3D silk/hydroxyapatite scaffolds for bone co-cultures. Adv Healthc Mater. 2012; 1:729–735. [PubMed: 23184824]
43. Aran K, Sasso LA, Kamdar N, Zahn JD. Irreversible, direct bonding of nanoporous polymer membranes to PDMS or glass microdevices. Lab Chip. 2010; 10:548–552. [PubMed: 20162227]

44. Wang Y, Kim YM, Langer R. In vivo degradation characteristics of poly(glycerol sebacate). J Biomed Mater Res A. 2003; 66:192–197. [PubMed: 12833446]

45. Pomerantseva I, Krebs N, Hart A, Neville CM, Huang AY, Sundback CA. Degradation behavior of poly(glycerol sebacate). J Biomed Mater Res A. 2009; 91:1038–1047. [PubMed: 19107788]

46. Chen QZ, Ishii H, Thouas GA, Lyon AR, Wright JS, Blaker JJ, et al. An elastomeric patch derived from poly(glycerol sebacate) for delivery of embryonic stem cells to the heart. Biomaterials. 2010; 31:3885–3893. [PubMed: 20153041]

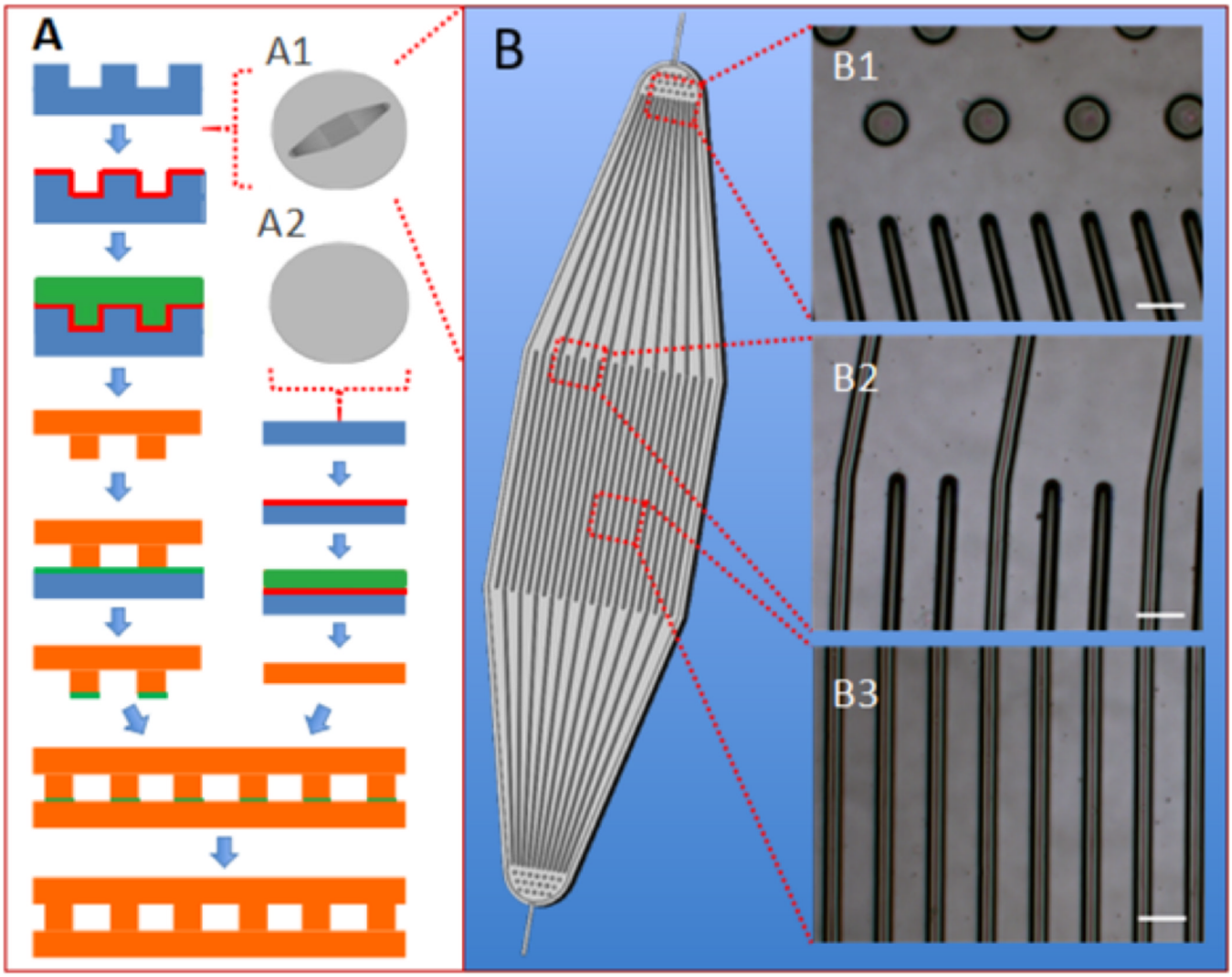

Figure 1.
Fabrication of PGS scaffolds from silicon wafers. (A) Assembly of a microfluidic device (μFD) base and thin membrane; (B) simplified schematic of the micropatterned wafer. (Insets A1 and A2) patterned and unpatterned wafers. (Insets B1–B3) light micrographs of μFD base showing transition from inlet posts to inlet channels (B1), transition from inlet region to central channels (B2), and central channels (B3). Silicon appears blue; maltose appears red; cured PGS appears orange, and PGS pre-polymer appears green. Scale bars: 100 μm.

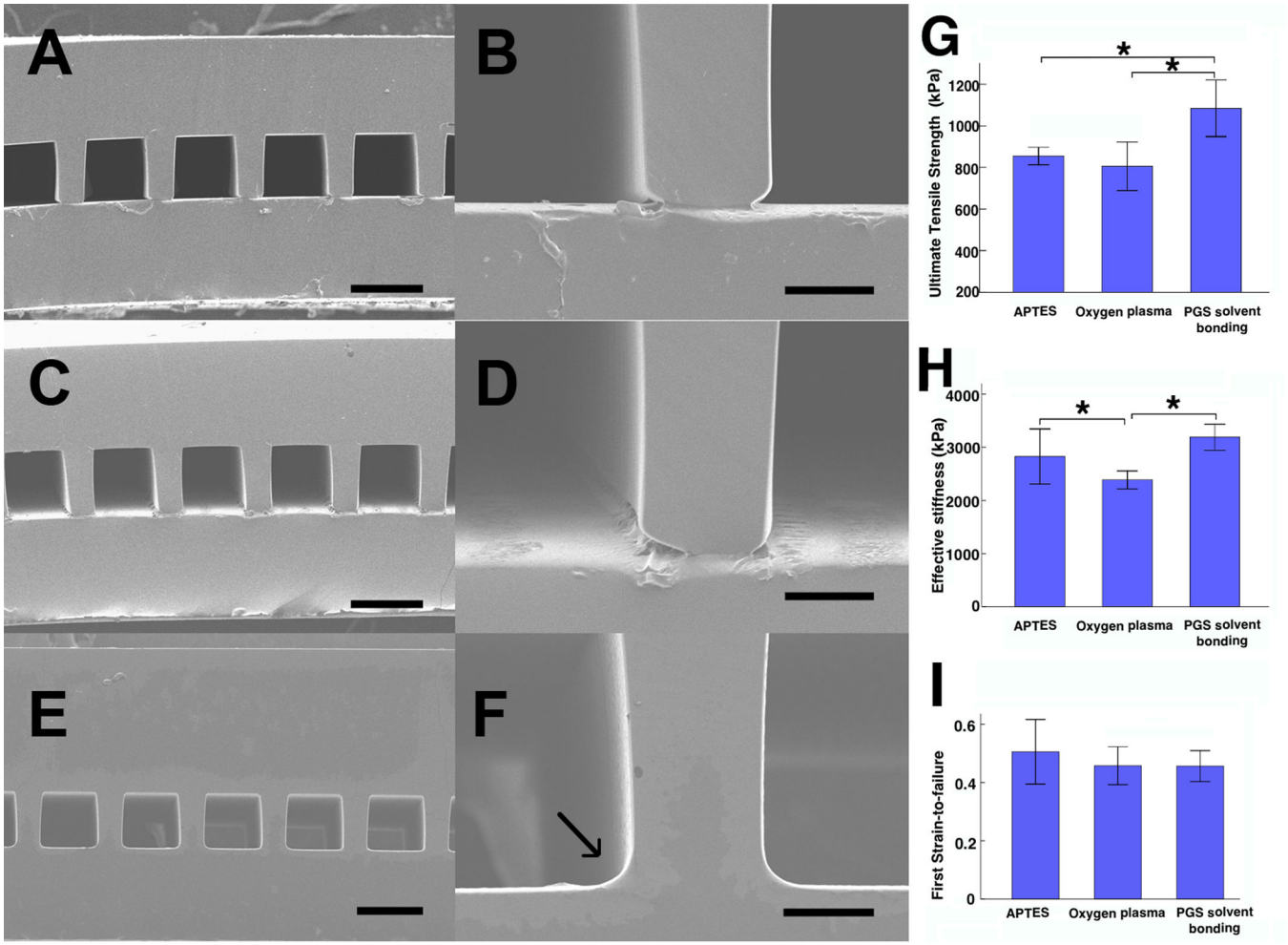

Figure 2.

Structural and mechanical properties of assembled scaffolds. (A–F) SEM images of scaffolds assembled by three methods (A, B) OP, (C, D) APTES and (E, F) PGS solvent bonding, which showed seamless binding (arrow) between the μFD base (above) and membrane (below). (G, H, I) Ultimate tensile stress (G), effective stiffness (H), and first strain-to-failure (I). Scale bars: (A, C, E) 100 μm, (B, D, F) 20 μm. Data are mean +/− SE. *Significant difference between groups.

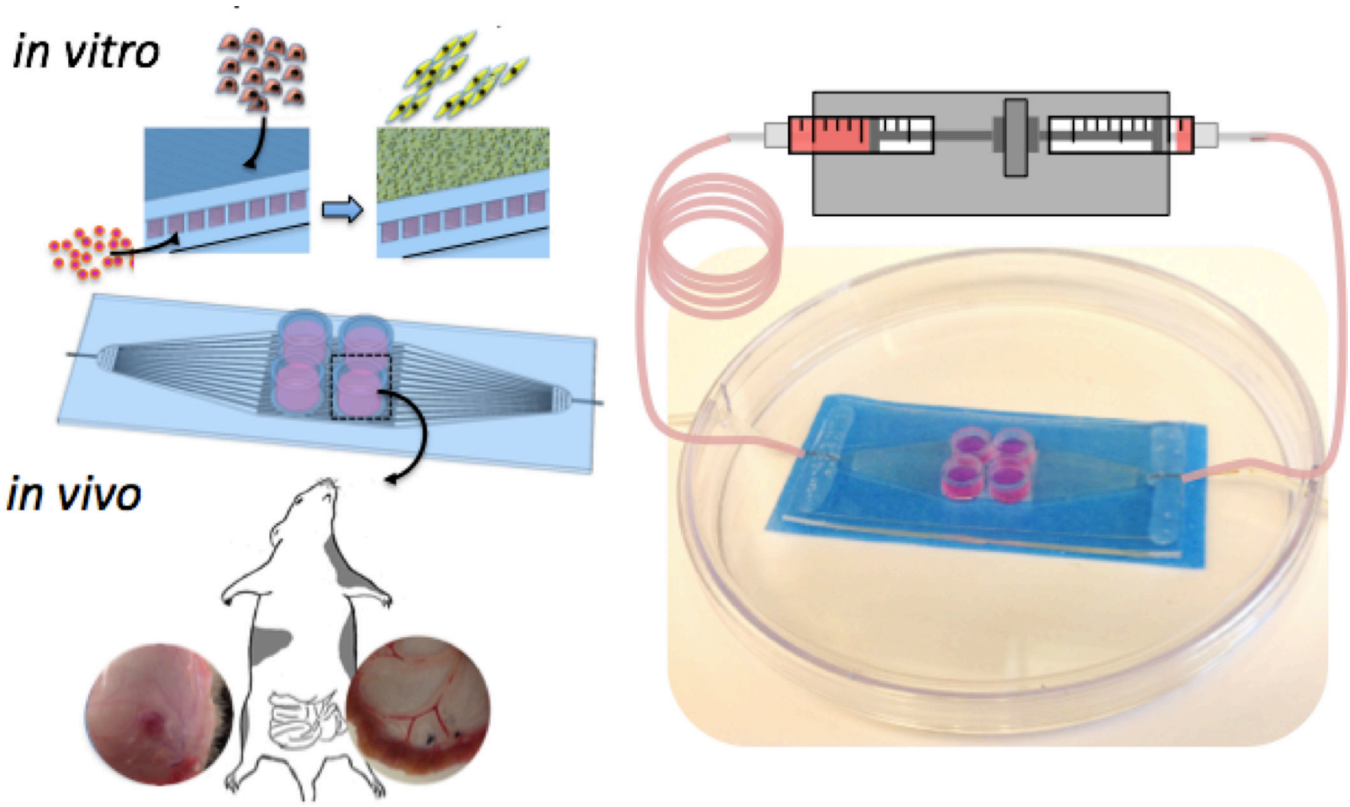

Figure 3.
Experimental designs. For some *in vitro* studies, human skeletal muscle derived cells were seeded in parenchymal spaces while microvessel perfusate was supplemented with a myotoxic drug (Doxorubicin); in other in vitro studies, microvessels were seeded with human umbilical vein endothelial cells. For *in vivo* studies, full-thickness punches of the scaffolds with or without both cell types were implanted subcutaneously or on the mesentery of the small intestine in nude rats.

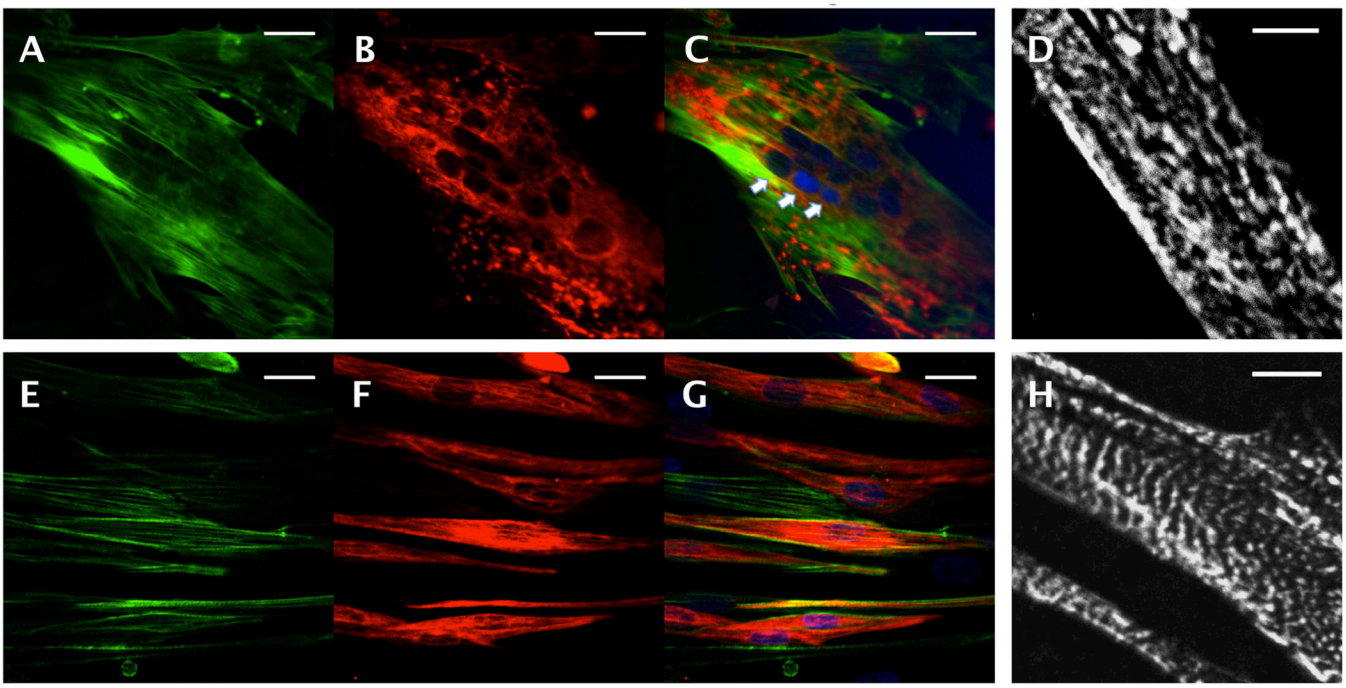

Figure 4.

Skeletal muscle cell differentiation on microvessel scaffolds. Confocal images of hSkMDCs (A–D) in the parenchymal space and (E–H) on glass coverslips; immunostaining for (A,E) F-actin (green), (B,F) desmin (red), (C,G) F-actin merged with desmin, with nuclear counterstain (blue), and (D,H) epifluorescence images after immunostaining for sarcomeric α-actin. Arrows point to a multi-nucleated cell. Scale bars: (A–C, E–G) 10 μm; (D, H) 5 μm.

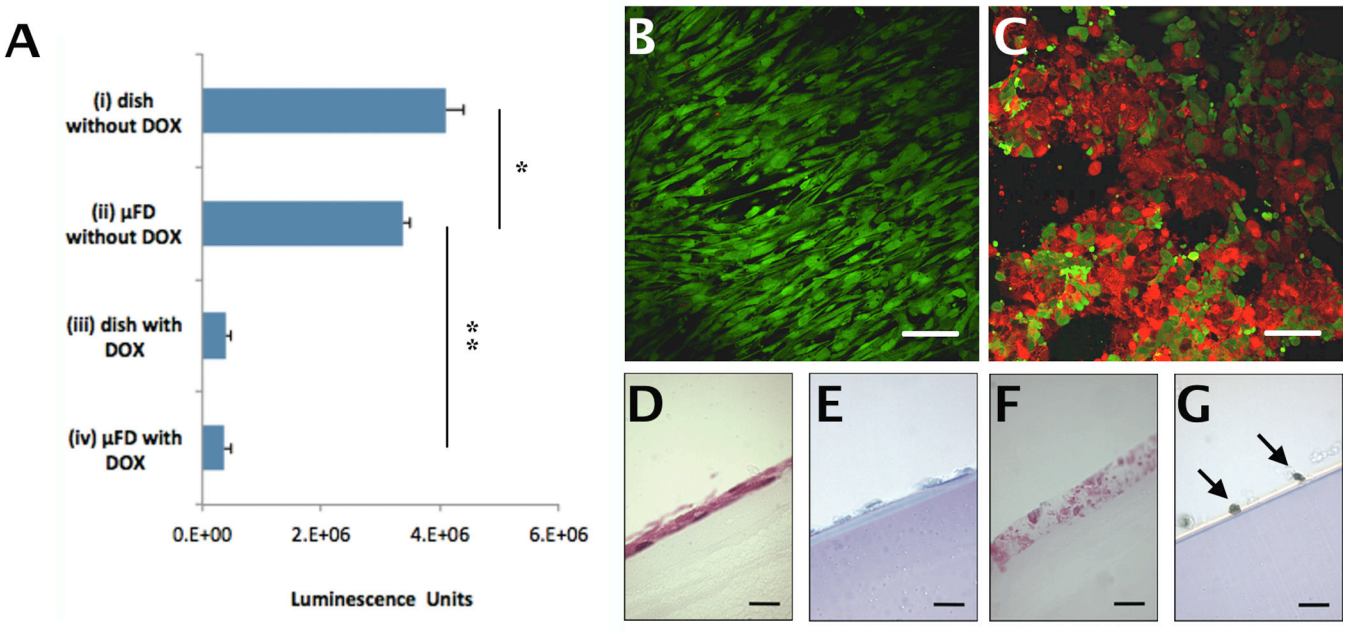

Figure 5.

Trans-membrane transport of a myotoxic drug from the microvessels to the parenchymal compartment. (A) Cell Titer-Glo™ viability data for four groups: (i) hSkMDCs on dish; no DOX in medium, (ii) hSkMDCs on scaffold; no DOX in perfusate; (iii) hSkMDCs on dish; DOX in medium, and (iv) hSkMDCs in scaffold; DOX in perfusate. (B, C) Epifluorescence images after live-dead staining of hSkMDCs in group ii (B) or group iv (C); live cells appear green, dead cells appear red. (D–G) Histological cross-sections of from group ii (D,E) and group iv (F,G) after staining with H&E (D,F) or TUNEL (E,G). Arrows (G) point to apoptotic nuclei. *Significant difference due to culture system (dish or scaffold); **Significant difference due to DOX. Scale bars: (B–C), 50 µm; (D–G), 25 µm.

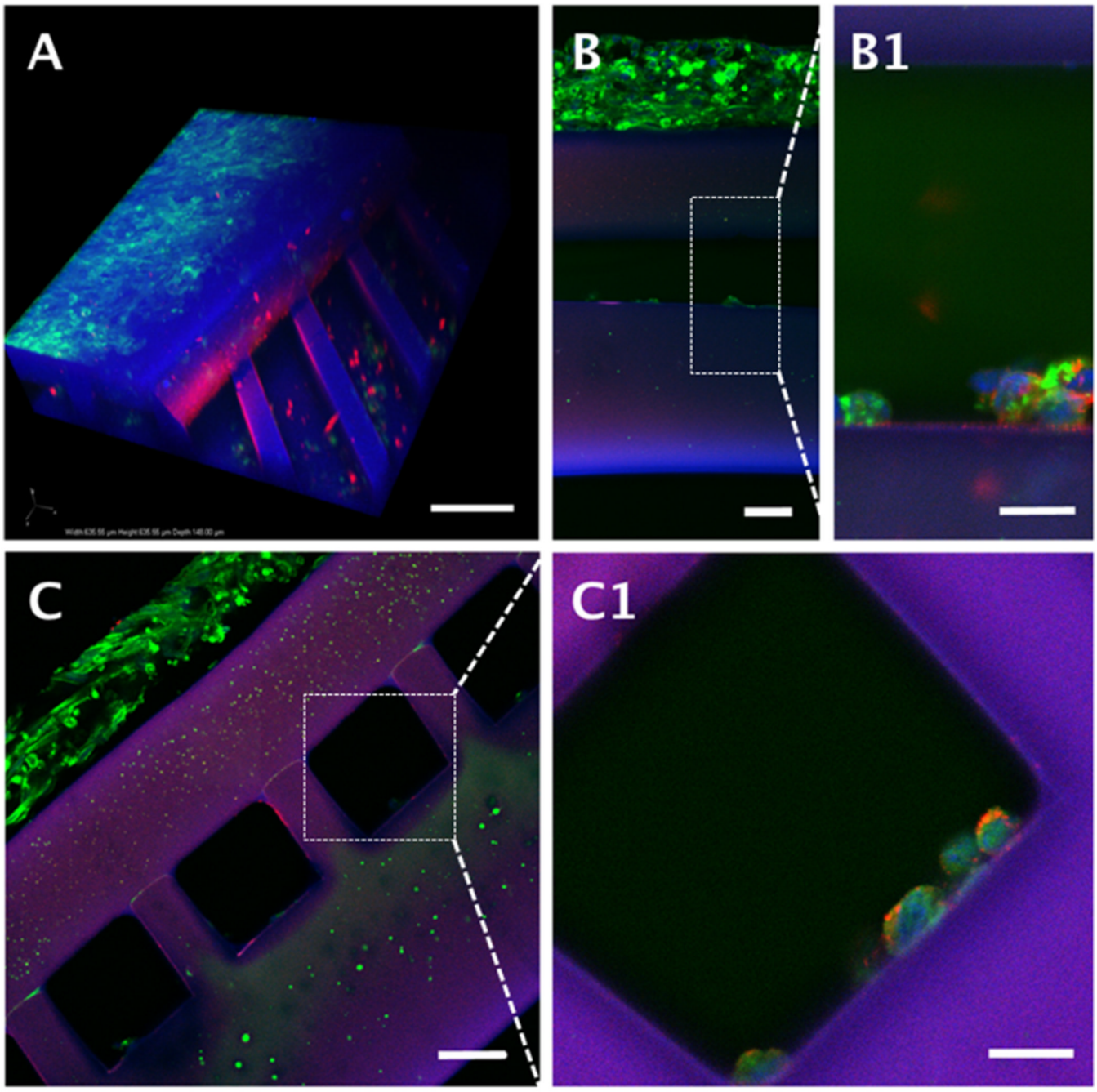

Figure 6.
Human umbilical vein endothelial cell seeding in microvessels of scaffolds with hSkMDCs cultured in parenchymal spaces. (A) 3-D confocal reconstruction; (B, C, Insets B1-C1) epifluorescence images of longitudinal sections (B, B1); and cross-sections (C, C1) after staining with von Willebrand's factor (red); F-actin (green) and nuclear counterstaining (blue); PGS appears blue-purple. Scale bars: (A) 100 μm; (B and C) 50 μm; (B1 and C1) 20 μm.

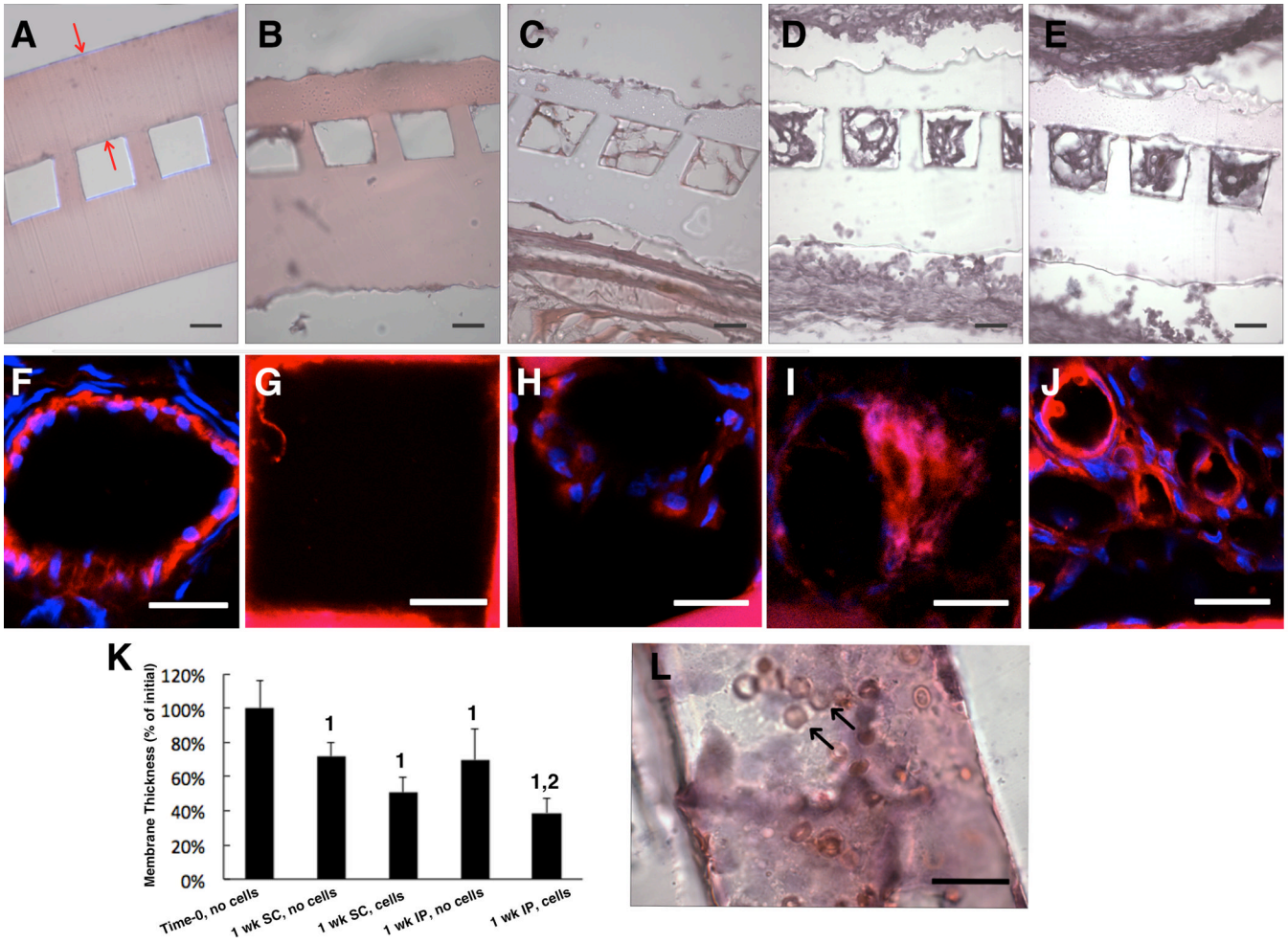

Figure 7.

Membrane biodegradation and microchannel vascularization *in vivo*. Initial (time-zero) implants are compared to explants in five groups: (A) Time-zero (B,C) one week subcutaneous (SC) explants without (B) or with (C) exogenous cells, (D,E) one week intraperitoneal (IP) explants without (D) or with exogenous (E,G) cells. (A-E,L) light micrographs of cross-sections (A-E) and a longitudinal section (L) stained with H&E. Confocal micrographs of a native blood vessel (F) and microvessels from SC scaffold without (G) or with (H) cells and IP scaffold without (I) and with (J) cells immunostained for anti-rat CD31. (K) membrane thickness expressed as % of initial; data are mean +/− SD. [1]Significant effect of time; [2]Significant effect of exogenous cells. (A) Red arrows show the membrane; (L) black arrows show red blood cells; (F–J) CD31 (and PGS) are red; cell nuclei are blue. Scale bars: (A–E) 50 μm; (G–L) 25 μm.

Table

Number of scaffolds per group that maintained mechanical integrity after perfusion at lower and higher flow rates for shorter and longer test periods.

Group	Number	10 (μ*L/min*)		100 (μ*L/min*)	
		4 h	120 h	4 h	120 h
Oxygen plasma	3	1	0	0	–
APTES	3	0	–	0	–
PGS Painting	3	3	3	3	3